Journal of Agricultural Engineering

https://www.agroengineering.org/

Optimisation of seasonal thermal energy storage capacity for greenhouse melon production using energy modelling

Sungwan Park,[1,2] Hoon Seonwoo[2,3]

[1]Smart Agriculture Major, Sunchon National University, Suncheon

[2]Department of Convergent Biosystems Engineering, College of Life Science and Natural Resources, Sunchon National University, Suncheon

[3]Interdisciplinary Program in IT-Bio Convergence System, Sunchon National University, Suncheon, South Korea

Corresponding author: Hoon Seonwoo, Department of Convergent Biosystems Engineering, College of Life Science and Natural Resources, Sunchon National University, 255 Jungang-ro, Suncheon 57922, South Korea. E-mail: uhun906@gmail.com

Please cite this article as doi: 10.4081/jae.2026.2191

Submitted: 19 March2026
Accepted: 19 August 2026

Optimisation of seasonal thermal energy storage capacity for greenhouse melon production using energy modelling

Sungwan Park,[1,2] Hoon Seonwoo[2,3]

[1]Smart Agriculture Major, Sunchon National University, Suncheon

[2]Department of Convergent Biosystems Engineering, College of Life Science and Natural Resources, Sunchon National University, Suncheon

[3]Interdisciplinary Program in IT-Bio Convergence System, Sunchon National University, Suncheon, South Korea

Corresponding author: Hoon Seonwoo, Department of Convergent Biosystems Engineering, College of Life Science and Natural Resources, Sunchon National University, 255 Jungang-ro, Suncheon 57922, South Korea. E-mail: uhun906@gmail.com

Contributions: Sungwan Park, methodology, software, conceptualization, investigation, formal analysis, writing – review and editing, writing – original draft, visualization, data curation. **Hoon Seonwoo**, supervision, conceptualization, methodology, project administration, funding acquisition, resources, writing – review and editing, validation. All the authors read and approved the final version of the manuscript and agreed to be accountable for all aspects of the work.

Conflict of interest: the authors declare no competing interests and all authors confirm accuracy.

Availability of data and material: The datasets used and/or analyzed during the current study are available upon reasonable request from the corresponding author.

Acknowledgements: Not applicable.

Funding: This work was partly supported by the Institute of Information & Communications Technology Planning & Evaluation (IITP)-Innovative Human Resource Development for Local Intellectualization program grant funded by the Korea government (MSIT)(IITP-2025-RS-2020-II201489, 35%) and the Institute of Information & Communications Technology Planning & Evaluation(IITP)-ITRC(Information Technology Research Center) grant funded by the Korea government(MSIT)(IITP-2025-RS-2023-00259703, 35%). This work was supported by project for Collabo R&D between Industry, University, and Research Institute funded by Korea Ministry of SMEs and Startups in 2025 (RS-2025-02314265, 30%).

Abstract

Carbon dioxide (CO_2), one of the major contributors to global warming and a factor affecting climate change, is predominantly emitted when fossil fuels are used to heat greenhouses during the winter season. Therefore, there is a need to implement adaptation of renewable energy to heat the greenhouses and reduce carbon emissions. In this study, the application of seasonal thermal energy storage (STES) using solar thermal energy (STE) sources in single and double-layered melon greenhouses was investigated with building energy simulation (BES). The double-layered greenhouse reduced the cumulative cooling load by 17.8% and the cumulative heating load by 61.6%, respectively, compared with the single-layered greenhouse, for which the cumulative cooling load was 42,714 MJ during the summer cropping season and the cumulative heating load was 36,531 MJ during the winter cropping season. Then, an STE-based STES system was developed and evaluated under various greenhouse conditions. When the STE-based STES system was applied to the melon greenhouse simulation, the required solar collector area and storage tank capacity for the double-layered greenhouse were 25–50% and 37–60% lower, respectively, than those required for the single-layered greenhouse. This study can contribute to the practical design of STES systems for melon greenhouses by providing a simulation-based method for estimating greenhouse heating demand and determining appropriate solar collector areas and storage tank capacities, thereby supporting sustainable agriculture by reducing fossil fuel consumption and mitigating greenhouse gas emissions.

Key words: greenhouse; melon; seasonal thermal energy storage; solar thermal energy; TRNSYS.

Introduction

Fossil fuels have been a major source of energy and a key driver of industrialization and economic growth since the Industrial Revolution (Höök and Tang, 2012). However, their combustion is also a major source of carbon dioxide (CO_2), contributing to global warming and climate change (Anwar *et al*., 2020; Filonchyk *et al.,* 2024). Global CO_2 emissions reached 36.8 billion tons in 2022, and the Intergovernmental Panel on Climate Change has emphasized that global carbon neutrality must be achieved by 2050 to limit the increase in global mean temperature to 1.5°C by 2100 (IEA, 2023; Allen *et al.*, 2018). Population growth and increasing food demand have led to the expansion of greenhouse cultivation worldwide (Esen and Yuksel, 2013). In January 2019, the global area used for greenhouse vegetable production was estimated at 496,800 ha (Roble, 2019). Because of their lightweight structures and intensive environmental control requirements, greenhouses often consume more fossil-fuel energy than similarly sized conventional buildings (Iddio *et al.*, 2020). In particular, greenhouse heating during winter depends heavily on fossil fuels, resulting in substantial CO_2 emissions (Hassanien *et al.*, 2016). Consequently, renewable energy systems are increasingly being investigated as alternatives for greenhouse heating and cooling. Several renewable energy technologies have been examined for greenhouse applications. Hussain *et al.* (2015) evaluated the thermal performance and economic feasibility of linear and spot Fresnel lens solar collectors for greenhouse heating. Kim *et al.* (2022) assessed the operating costs and greenhouse gas reduction potential of greenhouse systems using solar and geothermal energy. Attar *et al.* (2013) investigated the design parameters affecting the performance of solar greenhouse heating systems, whereas Aljubury and Ridha (2017) demonstrated the feasibility of a groundwater-assisted indirect-direct evaporative cooling system for greenhouse cooling. Together, these studies show that renewable energy technologies can contribute to more sustainable environmental control in protected cultivation. STE is a widely available renewable alternative to fossil fuels for greenhouse heating. However, its practical use is constrained by the seasonal mismatch between solar heat availability and greenhouse heating demand (Xu *et al.*, 2014). STES addresses this mismatch by storing STE during periods of low heating demand, such as spring, summer, and autumn, and supplying it during winter, when heating demand is high (Semple *et al.*, 2017; Dahash *et al.*, 2019; Adesanya *et al.*, 2025). STES systems can supply approximately 50-70% of annual heating demand and thereby reduce fossil fuel consumption (Fisch *et al.*, 1998). Semple *et al.* (2017) also evaluated solar collector designs for STES systems intended to meet annual greenhouse heating demand, demonstrating the importance of appropriately sizing both collection and storage components. Melon is an economically important horticultural crop in the Cucurbitaceae family and exhibits diverse agro-morphological and fruit characteristics (Kesh and Kaushik, 2021). Because melon requires relatively high temperatures for optimal growth and is increasingly cultivated in greenhouses, winter production relies substantially on fossil-fuel heating. Renewable energy-based heating systems are therefore needed to reduce carbon emissions from melon greenhouse production. However, their practical application requires accurate system sizing. The cooling and heating loads of the greenhouse must first be estimated so that renewable energy components can meet crop requirements without underdesign or overdesign (Lee *et al.*, 2017).

One of the major barriers to applying renewable energy systems in agriculture is the high initial installation cost. Therefore, accurate sizing of renewable energy systems for greenhouses is necessary to avoid overdesign, reduce unnecessary installation costs, and ensure that the system can meet the required heating and cooling loads (Park and Kim, 2019). Accurate predictions can reduce uncertainty in the initial and maintenance costs of renewable energy facilities, support system operators, and minimize disadvantages caused by deviations between predicted and actual performance (Antonanzas *et al.*, 2016). Greenhouse heating and cooling loads can be determined using either static or dynamic energy analysis. Static analysis assumes steady-state indoor and outdoor conditions and is generally used to size heating, ventilation, and air conditioning (HVAC) systems based on maximum load calculations. In contrast, dynamic analysis evaluates actual energy flows under non-steady-state conditions by considering the combined effects of conduction, convection, and radiation in response to changing weather variables, including wind direction, wind speed, solar radiation, solar position, and ambient temperature. Unlike static calculations, dynamic analysis can represent time-dependent variations in greenhouse energy demand and the interactions among multiple heat transfer processes. This approach is applied in building energy simulation (BES) to assess energy performance (Lee *et al.*, 2012). Although BES has traditionally been used in the architectural field, it has increasingly been adopted for agricultural applications (Lee *et al.*, 2016). The transient system simulation tool (TRNSYS, Ver. 18, USA), one of the widely used BES programs, supports greenhouse design and the development of microclimate control strategies for efficient energy management. By simulating the interactions among weather conditions, greenhouse structure, crop characteristics, and environmental control systems, TRNSYS can assist in evaluating greenhouse thermal performance and microclimate conditions (Xu *et al.*, 2014). Cam *et al.* (2024) developed a TRNSYS-based transient model integrating a photovoltaic-assisted heat pump HVAC system into a tomato greenhouse and showed that the system could regulate indoor temperature and humidity while reducing energy consumption and carbon emissions. Greenhouse heating and cooling loads are commonly estimated to determine the required capacities of heating and cooling systems. These calculations generally account for solar heat gains, convective heat transfer, ventilation and infiltration through openings and gaps, soil heat flux, and crop sensible and latent heat exchanges (Semple *et al*., 2017). Accordingly, a range of studies has applied BES and TRNSYS to predict greenhouse energy flows, evaluate thermal performance, and improve environmental control. Lee *et al*. (2016) developed and validated a real-time greenhouse energy exchange model for an apple mango greenhouse and analyzed the patterns of heating and cooling loads. Beaulac *et al*. (2024) developed a TRNSYS energy model for a small-scale greenhouse and improved its predictive accuracy through calibration and validation using measured data, thereby confirming the reliability of the modeling approach. Rasheed *et al.* (2020) proposed a BES model for estimating annual and maximum greenhouse heating loads and simulating greenhouse microclimate conditions. Their study also assessed the thermal performance of greenhouse covering materials and energy-saving screens. Adesanya *et al*. (2025) evaluated a hybrid renewable energy system combined with thermal energy storage for a net-zero-energy tomato greenhouse. Their results indicated that optimized integration of solar photovoltaic energy and thermal energy storage could improve energy self-sufficiency, stabilize greenhouse operation under fluctuating environmental conditions, and provide a practical pathway toward sustainable greenhouse production. Other studies have focused on specific greenhouse thermal characteristics and heating demand. Rabiu *et al*. (2022) estimated the overall heat transfer coefficient of an energy-saving screen by combining TRNSYS simulations with hotbox experiments, thereby contributing to improved evaluation of greenhouse covering insulation. Ha *et al*. (2015) used a validated greenhouse model to analyze heating characteristics and predict maximum and annual heating loads according to greenhouse type and location. Ahamed *et al*. (2020) modeled a Chinese-style solar greenhouse for year-round cultivation in high-latitude regions and analyzed its heating demand under controlled environmental conditions. Collectively, these studies demonstrate that BES and TRNSYS provide effective tools for estimating greenhouse energy loads, evaluating thermal characteristics, and designing renewable energy and thermal storage systems under a wide range of operating conditions. Research has been conducted on the cooling and heating loads of greenhouses for some crops, such as tomato and strawberry. Çam *et al*. (2024) developed a TRNSYS-based transient model integrating a photovoltaic-assisted heat pump HVAC system to control the indoor temperature and humidity of a tomato greenhouse while reducing energy consumption and carbon emissions. Ogunlowo *et al*. (2023) integrated a strawberry growth model into a

TRNSYS-based greenhouse model to simultaneously simulate greenhouse energy consumption and strawberry yield. In addition, Zhang *et al*. (2015) used TRNSYS to design and optimize a low-cost seasonal solar soil heat storage system for greenhouse heating by analyzing the depth and number of U-pipes and the solar collector configuration. However, research specifically focused on determining the cooling and heating loads of melon greenhouses remains limited. Moreover, few studies have integrated melon growth-stage-specific environmental requirements with greenhouse energy load estimation and STE-based STES capacity design. Therefore, this study was conducted to estimate the cooling and heating loads of melon greenhouses and determine an appropriate capacity for an STE-based STES system for winter heating.

The overall objective of this study was to determine the appropriate capacity of a STE-based STES system for melon greenhouses by linking crop growth-stage-specific environmental requirements, greenhouse energy load analysis, and STES design (Figure 1) (Park, 2023). Specifically, this study aimed to: i) develop TRNSYS-based energy models for single- and double-layered melon greenhouses by using BES; ii) estimate and compare the cooling and heating loads of the two greenhouse types by considering melon growth-stage-specific temperature settings, greenhouse physical properties, crop growth data, and weather data; iii) determine the required solar collector area and storage tank volume of the STE-based STES system under different storage tank heat loss coefficients; and iv) evaluate the integrated greenhouse–STES model to determine whether the selected STES capacity can satisfy the winter heating demand and to examine the effect of pump flow rate on heat supply. The results of this study are expected to support the design of efficient renewable energy-based heating systems for melon greenhouses and contribute to reducing fossil fuel consumption and greenhouse gas emissions in protected horticulture.

Materials and Methods

Model specification

To estimate the heating and cooling loads of a melon greenhouse, a greenhouse model was designed with three components: the greenhouse structure, crops, and BES software. The greenhouse model allowed for a comprehensive analysis of the energy in the system and estimation of the heating and cooling loads.

Greenhouse model

The greenhouses used in this study consisted of single- and double-layered greenhouse models provided by the Rural Development Administration (RDA) of South Korea. Figure S1 shows the single- and double-layered greenhouse models. The single-layered greenhouse had a length of 35 m, a width of 7 m, a ridge height of 3.9 m, an eaves height of 2 m, and a volume of 744.97 m^3. The double-layered greenhouse had a length of 31.6 m, a width of 8.9 m, a ridge height of 3.9 m, an eaves height of 1.7 m, and a volume of 850.53 m^3. The greenhouse covering consisted of polyethylene (PE) film with a thickness of 0.1 mm. The greenhouse specifications are presented in Table S1, while the physical properties of the wall and floor materials, based on Lee *et al*. (2012), are presented in Table 1. The properties of the covering materials, based on Lee *et al*. (2016), are presented in Table 2.

Crop model

Melon was chosen as the model crop, and the cropping season was set from May 24 to August 31 for the summer season and from September 23 to December 31 for the winter season. During each cropping season, the leaf area index (LAI) of the crop was set to increase from 0.02 to 2.8. Table S2 shows the growth data of the melons during one cropping season. The heating and cooling temperature settings of the greenhouse were divided into four stages based on the growth stage of the melon. The temperature for stage 1, the period from planting to fruit bearing, was set at 14°C for heating and 28°C for cooling. At stage 2, which represents the fruit growing period, the temperature was set at 18°C for heating and 28°C for cooling. At stage 3, the fruit net growing period, the temperature was set at 18°C for heating and 35°C for cooling. At stage 4, which represents the period from maturation to harvesting, the temperature was set at 14°C for heating and 28°C for cooling. These temperature settings are summarized in Table 3.

Crop sensible and latent heat exchanges were calculated using the crop energy exchange equations proposed by Stanghellini (1987). The sensible heat exchange between the crop canopy and greenhouse air was calculated from the temperature difference between the leaf surface and the greenhouse air, as shown in Equation (1). The latent heat exchange caused by crop transpiration was calculated from the vapor pressure difference between the leaf surface and greenhouse air, as shown in Equation (2).

$$H = \frac{2LAI\rho_a C_p (T_L - T_a)}{r_e} \quad \text{(Eq. 1)}$$

$$LE = \frac{2LAI\rho_a C_p}{\gamma (r_i + r_e)} (e_E - e_a) \quad \text{(Eq. 2)}$$

Where: H is the sensible heat exchange of the crop canopy (W/m^2); LE is the latent heat exchange of the crop canop y(W/m^2), LAI is the leaf area index; ρ_a is the air density () (kg/m^3); C_p is the specific heat capacity of air ($J/(kg \cdot °C)$); T_L is the leaf temperature (°C); T_a is the greenhouse air temperature (°C); r_e is the boundary layer resistance for heat and water vapor transfer *(s/m)*; r_i is the stomatal resistance *(s/m)*; γ is the psychrometric constant (*Pa*/°C); e_E is the saturation vapor pressure at the leaf surface (*Pa)*; and e_a is the actual vapor pressure of the greenhouse air (*Pa)*.

The auxiliary variables required to calculate crop sensible and latent heat exchanges were estimated using Equations (3)–(7). The leaf-air temperature difference was calculated as a function of incident solar radiation on the crop canopy, internal wind speed, and vapor pressure difference, as shown in Equation (3). The boundary layer resistance was calculated using leaf length, leaf-air temperature difference, and internal wind speed, as shown in Equation (4). The vapor pressure difference between the leaf surface and greenhouse air was calculated from the saturation vapor pressure and relative humidity of the greenhouse air, as shown in Equation (5). The saturation vapor pressure of the greenhouse air and the psychrometric constant were calculated using Equations (6) and (7), respectively (Stanghellini, 1987; Jabloun and Sahli, 2008; Goo *et a*l., 2021; Nam *et al.*, 2024).

$$(T_L - T_a) = 0.0018R_n + 0.6470u - 1.2757(e_E - e_a) \quad \text{(Eq. 3)}$$

$$r_e = \frac{1174l^{0.5}}{(l|T_L - T_a| + 207u^2)^{0.25}} \quad \text{(Eq. 4)}$$

$$(e_E - e_a) = VP_{air}\left(1 - \frac{H_{air}}{100}\right) \quad \text{(Eq. 5)}$$

$$VP_{air} = 610.7 \times 10^{\frac{7.5T_a}{237.3+T_a}}$$ (Eq. 6)

$$\gamma = 0.665 \times 10^{-3} P$$ (Eq. 7)

Where: T_L - T_a is the leaf-air temperature difference (°C); R_n is the incident solar radiation on the crop canopy (W/m^2); u is the wind speed inside the greenhouse *(m/s)*; $e_E - e_a$ is the vapor pressure difference between the leaf surface and greenhouse air (Pa); r_e r_e the boundary layer resistance for heat and water vapor transfer *(s/m)*; l is the characteristic leaf length (*m*); VP_{air} is the saturation vapor pressure of the greenhouse air at T_a T_a (Pa); H_{air} is the relative humidity inside the greenhouse (%); γ is the psychrometric constant (*Pa*/°C); and P is the atmospheric pressure (*Pa*).

The stomatal resistance of the crop canopy was calculated using the model proposed by Stanghellini (1987). In this model, the stomatal resistance is expressed as the product of the minimum stomatal resistance and dimensionless correction factors representing the effects of solar radiation, leaf temperature, CO_2 concentration, and vapor pressure difference, as shown in Equation (8). The correction factors for incident solar radiation and leaf temperature were calculated using Equations (9) and (10), respectively. The effect of CO_2 concentration on stomatal resistance was calculated using Equation (11), with the conditional limits shown in Equation (12). The effect of vapor pressure difference between the leaf surface and greenhouse air was calculated using Equation (13), with the conditional limits shown in Equation (14). The parameter values used in these equations are listed in Table 6.

$$r_i = r_{min} \bullet \tilde{r}_i(R_n) \bullet \tilde{r}_i(T_0) \bullet \tilde{r}_i(CO_2) \bullet \tilde{r}_i(e_E - e_a)$$ (Eq. 8)

$$\tilde{r}_i(R_n) = \frac{R_n + C_1}{R_n + C_2}$$ (Eq. 9)

$$\tilde{r}_i(T_0) = 1 + C_3(T_L - T_m)^2$$ (Eq. 10)

$$\tilde{r}_i(CO_2) = 1 + C_4(CO_2 - 200)^2 \quad \text{(Eq. 11)}$$

$$f(x) = \begin{cases} 1, \; R_n = 0 W \bullet m^{-2} \\ 1 + 6.1 \times 10^{-7}(CO_2 - 200)^2, \; CO_2 < 1100 vpm \\ 1.5, \; CO_2 \geq 1100 vpm \end{cases} \quad \text{(Eq. 12)}$$

$$\tilde{r}_i(e_E - e_a) = 1 + C_5(e_E - e_a)^2 \quad \text{(Eq. 13)}$$

$$f(x) = \begin{cases} 1 + 4.3(e_E - e_a)^2, \; e_E - e_a < 0.8\, kPa \\ 3.8, \; e_E - e_a \geq 0.8\, kPa \end{cases} \quad \text{(Eq. 14)}$$

Where: r_i is the stomatal resistance of the crop canopy (s/m); r_{min} is the minimum stomatal resistance (s/m); $\widetilde{r_i}(R_n)$, $\widetilde{r_i}(T_0)$, $\widetilde{r_i}(CO_2)$, and $\widetilde{r_i}(e_E - e_a)$ are dimensionless correction factors for incident solar radiation, leaf temperature, CO_2 concentration, and vapor pressure difference, respectively; R_n is the incident solar radiation on the crop canopy (W/m^2); T_L is the leaf temperature (°C); T_m is the reference leaf temperature for stomatal response (°C); CO_2 is the carbon dioxide concentration in the greenhouse air (*vpm*); e_E–e_a is the vapor pressure difference between the leaf surface and greenhouse air (*kPa*); and C_1, C_2, C_3, C_4 and C_5 are empirical coefficients listed in Table 4.

BES software

BES is a program used to calculate heat and energy flows in buildings and determine the energy loads required for optimal environmental control. TRNSYS was a BES program developed for dynamic simulation and solar thermal system modeling, which could consider various factors such as outdoor conditions, solar radiation, wall properties, indoor temperature and humidity, and ventilation rate in real time to provide a sufficient amount of quantitative data for comparative analysis within a short time (Lee *et al.*, 2012). TRNSYS effectively performed dynamic thermal energy analysis of buildings by connecting various components centered around the multi-zone building component, and equation (15) represented the complex heat transfer processes occurring within such buildings (Lee *et al*., 2017; Transsolar Energietechnik GmbH, 2019; Ahamed *et al*., 2020).

$$Q_i = Q_{surf,i} + Q_{inf,i} + Q_{vent,i} + Q_{g,c,i} + Q_{cplg,i} + Q_{solair,i} + Q_{ISHCCI,i} \quad \text{(Eq. 15)}$$

Where: Q_i is the heat flux of the zone; $Q_{surf,i}$ is the convective gain from surfaces; $Q_{inf,i}$ is the infiltration gain; $Q_{vent,i}$ is the ventilation gain; $Q_{g,c,i}$ is the internal convective gain; $Q_{cplg,i}$ is the gain due to air flow from airnode or boundary condition; $Q_{solair,i}$ is the fraction of solar radiation entering an airnode through external windows; and $Q_{ISHCCI,i}$ is the absorbed solar radiation directly transferred as convective gain to internal air.

For the design of the greenhouse energy model using TRNSYS, the meteorological data of Gwangju Metropolitan City provided by the Korea Meteorological Administration were used. The greenhouse and crop components were integrated into the TRNSYS program. The single-layered and double-layered greenhouse models were applied to the multi-zone building component to calculate the heating and cooling loads. TRNSYS components and their descriptions are shown in Table S3.

STES model

Tank Thermal Energy Storage (TTES) was used as part of the STES system. TTES used water as a storage medium to provide high energy density and large heat capacity. It utilized temperature stratification to increase the efficiency of heat transfer within the water and minimize water losses. By maintaining a specific temperature range through temperature stratification, temperature fluctuations could be minimized and consistent temperature levels could be achieved. TTES offered design flexibility and ease of maintenance (Dahash *et al*., 2019; Trier, 2012). Like the BES model, this was a model of the STES system using TRNSYS. The components used in the STES model included a data reader, equation, solar radiation processor, psychrometrics component, solar collector, storage tank, pump, controller, and load, with their detailed descriptions and corresponding parameter values presented in Tables S3 and S4, respectively. Notably, the thermal storage tank loss coefficient of 0.3 kJ/h·m²·K represents a tank wall constructed with 0.5 m thick glass wool insulation and 0.005 m thick stainless steel (Chung *et al.*, 1998). In this study, the storage tank loss coefficient of 0 kJ/h·m²·K was used as an ideal reference case rather than a practical storage tank condition. This assumption was applied to estimate the theoretical minimum STES capacity and to isolate the effect of storage tank heat loss on the required solar collector area and storage tank volume. To consider more realistic storage tank conditions, additional loss coefficients of 0.3, 0.5, 1.0, 1.5, and 2.0 kJ/h·m²·K were also applied. The control of the STES system worked as follows: from January 1 to September 22 (0-6359 h), when the solar collector outlet temperature was at least 10°C higher than the storage tank nodal temperature, the pump operated to store heat in the storage tank, and it stopped when the temperature difference decreased to 2°C; the high-limit cut-out temperature was set to 80°C. From September 23 to December 31 (6360~8760 h), the heat stored in the storage tank was used to heat the greenhouse. The heating load data obtained from the greenhouse model was applied to the designed STES model to select the capacity of the solar collector and storage tank according to the loss coefficient of the thermal storage tank.

Greenhouse and STES-combined model

A greenhouse and STES-combined model was developed using TRNSYS, in which the STES was connected to the greenhouse through a heat exchanger component, whose specifications are presented in Table S4. The components used in this model were the same as those used in the greenhouse model and the STES model. The description and input values for the components are shown in Tables S3 and S4. The STES model with a storage tank loss coefficient of 0 kJ/h·m²·K was combined with the single-layered greenhouse model to verify that the selected STES capacity met the heating load of the greenhouse model and to check the ratio of the greenhouse heating load according to the pump capacity. The greenhouse heating load ratio was calculated by dividing the accumulated value of the heat energy exchanged in the heat exchanger by the accumulated value of the greenhouse heating load and multiplying by 100. To assess the STES capacity selected from the STES model, the ranges of solar collector area and storage tank volume were extended to 10–60 m^2 and 50–300 m^3, respectively, and the greenhouse heating load ratio was evaluated. To determine the pump capacity, the solar collector area was fixed at 20 m², the storage volume ranged from 50 to 300 m³, and the pump flow rate varied from 500 to 5000 kg/h. In addition, changes in the flow rate according to the growth stage of the crop were considered, with flow rates of 500, 1000, 4000, 3000 kg/h and 500, 2000, 4000, 4000 kg/h, respectively, to check the greenhouse heating load ratio. Furthermore, the greenhouse heat load ratio was compared while varying the solar collector area and storage tank volume when the flow rate was varied according to the crop growth stage (500, 1000, 4000, 3000 kg/h) and when the pump flow rate was kept constant at 5000 kg/h.

Results and Discussion

Greenhouse model

As shown in Figure 2A, a greenhouse thermal energy calculation model was created using weather data and crop data, and various components such as data reader to read data files, equation to apply evapotranspiration equation of crops, solar radiation, psychrometrics, sky temperature to convert weather data to multi-zone building, multi-zone building to apply data from greenhouse to calculate heating and cooling load data, and online plotter to output calculated heating and cooling load data. Table 5 presents the annual cumulative cooling and heating loads, growth-stage-specific loads, and maximum hourly loads with their occurrence dates for the single- and double-layered greenhouses during 2017–2022. Figure 2B compares the cumulative cooling load between the single-layered greenhouse and the double-layered greenhouse during the summer cropping season from 2017 to 2022. The cooling load of the double-layered greenhouse was reduced by 17.8% compared to the single-layered greenhouse. To evaluate the uncertainty associated with interannual weather variability, the cooling load was summarized using the mean, standard deviation, and minimum–maximum range. The cumulative cooling load of the single-layered greenhouse was 42,714 ± 7,666 MJ, with a range of 36,970–57,258 MJ, whereas that of the double-layered greenhouse was 35,108 ± 6,163 MJ, with a range of 30,191–46,727 MJ. The maximum cumulative cooling load occurred in 2018, with 57,258 MJ for the single-layered greenhouse and 46,727 MJ for the double-layered greenhouse. There were no heating loads during the summer cropping season. Figure 2C compares the cumulative heating and cooling loads between the single-layered greenhouse and the double-layered greenhouse during the winter cropping season from 2017 to 2022. The heating load of the double-layered greenhouse was reduced by 61.6% and the cooling load was reduced by 5.3% compared to the single-layered greenhouse. The winter cumulative cooling load of the single-layered greenhouse was 6,801 ± 996 MJ, with a range of 5,113–8,173 MJ, whereas that of the double-layered greenhouse was 6,443 ± 1,052 MJ, with a range of 4,956–7,905 MJ. The winter cumulative heating load of the single-layered greenhouse was 36,531 ± 3,235 MJ, with a range of 32,151–41,577 MJ, whereas that of the double-layered greenhouse was 14,011 ± 2,021 MJ, with a range of 11,714–17,012 MJ. The maximum cumulative cooling loads occurred in 2021 at 8,173 MJ for the single-layered greenhouse and 7,905 MJ for the double-layered greenhouse. The maximum cumulative heating loads occurred in 2017, with 41,577 MJ for the single-layered greenhouse and 17,012 MJ for the double-layered greenhouse. These results indicate that interannual weather variability affected the cooling and heating energy demand of the melon greenhouses.

Figures S2 and S3 show the annual cooling and heating loads of the greenhouse according to the set temperature for each melon growth stage and the ambient temperature during 2017-2019 and 2020-2022, respectively. For the single-layered greenhouse, the observed maximum heating load over the six years was 88.52 MJ/h and the maximum cooling load was 143.26 MJ/h, with the occurrence dates of December 9, 2018 and May 24, 2022, respectively. During the six-year summer cropping season, the average cumulative cooling load per growth stage was 24,205 MJ for stage 1, 3,603 MJ for stage 2, 5,058 MJ for stage 3, and 9,845 MJ for stage 4. There was no heating load during the six-year summer cropping season. During the six-year winter cropping season, the average cumulative cooling load per growth stage was 6,788 MJ for stage 1, 35 MJ for stage 2, and none for stages 3 and 4. The maximum cumulative heating load was 17,011 MJ in 2017 and the maximum cumulative cooling load was 46,727 MJ in 2018.

The differences in energy loads between single-layered and double-layered greenhouses were clearly identified. The double-layered greenhouse showed a 17.8% reduction in cooling load and a 61.6% reduction in heating load compared to the single-layered greenhouse. These differences are attributed to the insulation effect provided by the double-layered structure, which has a particularly significant impact on heating load reduction. Similar energy-saving effects of double-layered covered greenhouses have been reported in the study by Abbouda *et al.* (2012), and our results support these findings. Furthermore, the double-layered structure creates an additional air layer between the inner and outer layers that acts as an insulator, reducing heat transfer. Analysis of energy loads by melon growth stage revealed that heating loads were highest during Stage 3 (fruit net growing period) and Stage 4 (maturation to harvesting). This can be attributed to the lower external temperatures during winter combined with the higher set temperature (18°C) required during these periods. These results suggest the need for additional insulation or alternative energy systems, particularly for Stages 3 and 4, to ensure efficient energy management. Additionally, analysis of six years of data confirmed that maximum heating loads and cooling loads occurred in 2017 and 2018, respectively. This demonstrates the impact of annual climate variability on greenhouse energy requirements and suggests that long-term energy planning should consider the effects of climate change. The influence of annual climate variations on greenhouse energy loads was also emphasized in the study by Trépanier *et al*. (2024), and our research confirms this for melon cultivation greenhouses.

STES model

The STES simulation results indicated the solar collector area and storage tank volume required to meet the greenhouse heating load during the winter cropping season. Figure 3A shows the STES model using TRNSYS to calculate the area of the solar collector and the volume of the storage tank. The heating load data from 2017, which showed the maximum cumulative heating load in the greenhouse model, was used as the load. To determine the capacity of the solar collector and the storage tank, the area of the solar collector was gradually increased, and the volume of the storage tank was gradually increased to find the volume corresponding to the heating load. Then, with the determined storage tank volume, the area of the solar collector was gradually increased to find the area matching the heating load. In addition, the capacity of the solar collector and the storage tank was calculated by varying the loss coefficient of the storage tank. Figure 3B shows the flow chart of the STES model. From January 1 to September 22, before the start of the winter cropping season, when the temperature of the storage tank was lower than the temperature of the solar collector, the pump (solar collector) was operated to store heat in the storage tank. From September 23 to December 31, during the winter cropping season, the pump (load) was operated to deliver the heat stored in the storage tank to the load. Figure 4A shows the STES capacity according to the variation of the loss coefficient of the storage tank by examining the average temperature of the storage tank and the difference between the input and loss energy in the STES model using the heating load of the single-layered greenhouse. On the left, the average temperature of the storage tank was kept at 20°C on December 31, assuming it was 20°C on January 1, and the capacities of the solar collector and the storage tank were determined. On the right, the capacities of the solar collector and the storage tank were determined when the accumulated difference between the input and loss energy of the storage tank until December 31 was higher than the accumulated heating load. When the loss coefficient was 0 kJ/h·m^2·K, the area of the solar collector was 30 m^2 and the volume of the storage tank was 200 m^3, which satisfied the heating load. The selected capacities of solar collectors and storage tanks according to the loss coefficient were as follows (loss coefficient (kJ/h·m^2·K) - solar collector area (m^2) - storage tank volume (m^3)): 0-30-200, 0.3-40-200, 0.5-40-250, 1.0-60-300, 1.5-90-350, 2.0-130-400. Figure 4B shows the STES capacity according to the variation of the storage tank loss coefficient by examining the average storage tank temperature and the difference between the input and loss energy in the STES model using the heating load of the double-layered greenhouse. On the left, the average temperature of the storage tank was kept at 20°C on December 31, assuming it was 20°C on January 1, and the capacities of the solar collector and the storage tank were determined. On the right, the capacities of the solar collector and the storage tank were determined when the accumulated difference between the input and loss energy of the storage tank until December 31 was higher than the accumulated heating load. When the loss coefficient was 0 kJ/h·m^2·K, the area of the solar collector was 20 m^2 and the volume of the storage tank was 100 m^3, which satisfied the heating load. The selected capacities of solar collectors and storage tanks according to the loss coefficient were as follows (loss coefficient (kJ/h·m^2·K) - solar collector area (m^2) - storage tank capacity (m^3)): 0-20-100, 0.3-20-100, 0.5-30-100, 1.0-40-150, 1.5-50-200, 2.0-70-250.

Table 6 presents whether the energy charged into the STES system satisfied the heating demand of the single-layered and double-layered greenhouses according to the storage tank loss coefficient, solar collector area, and storage tank volume. It was confirmed that the demand was satisfied when the difference between the input and loss energies of the storage tank exceeded the heating load. As the storage tank loss coefficient increased, the solar collector area and storage tank volume of the STES increased due to the increase in energy loss from the storage tank. In addition, the solar collector area decreased by 25-50% and the storage tank volume decreased by 37-60% in the case of double-layered greenhouse compared with single-layered greenhouse. Therefore, application of the STES system to double-layered greenhouse enables the installation of a smaller capacity system compared to single-layered greenhouse.

Design parameters for STES systems to meet greenhouse heating demands were derived. A particularly notable finding is the impact of storage tank insulation performance on the overall scale of the STES system. As the loss coefficient increased from 0 kJ/h·m²·K to 2.0 kJ/h·m²·K, the required solar collector area significantly increased from 30 m² to 130 m² for single-layered greenhouses and from 20 m² to 70 m² for double-layered greenhouses. This empirically supports the importance of insulation in STES systems as presented by Dolgun *et al.* (2023). The insulation treatment of the storage tank directly affects system efficiency, suggesting that a balance between initial investment costs and long-term operational costs should be considered. For practical implementation, the insulation type and thickness should be selected by considering local climatic conditions, available space, and economic constraints. Additionally, the STES system required for double-layered greenhouses was found to be considerably smaller than that for single-layered greenhouses. The solar collector area decreased by approximately 25-50%, and the storage tank volume decreased by approximately 37-60%. This is directly attributed to the reduced heating load due to the enhanced insulation properties of double-layered greenhouses. From an economic perspective, the combination of a double-layered greenhouse and a smaller STES system may be advantageous in terms of initial investment costs compared to a single-layered greenhouse with a larger STES system. However, the additional cost of the double-layered greenhouse structure itself must also be considered. Therefore, a comprehensive life cycle cost analysis should be conducted in future research.

Greenhouse and STES-combined model

The STES model incorporating a storage tank loss coefficient of 0 kJ/h·m²·K was integrated with the single-layered greenhouse model to assess whether the selected STES capacity could fulfill the heating demand of the greenhouse and to evaluate the ratio of the greenhouse heating load as a function of the pump capacity. Figure 5A shows a model combining the greenhouse and the STES using TRNSYS, where the storage tank of the STES is connected to the greenhouse through a heat exchanger. Figure 5B shows the flow chart of the combined model. From January 1 to September 22, heat is stored in the storage tank. When the temperature of the solar collector is higher than the temperature of the storage tank, pump 1 is operated to charge the storage tank with the heat collected from the solar collector. During the winter cropping season from September 23 to December 31, heat is stored in the storage tank and the stored heat is also used to heat the greenhouse. When the greenhouse temperature is lower than the storage temperature and the set heating temperature, the stored heat is transferred to the greenhouse. Figure 6A shows the ratio of greenhouse heating load according to solar collector area and storage tank volume, which was used to evaluate the STES capacity. The pump flow rate was set to 3000 kg/h. It was confirmed that when the solar collector area was larger than 20 m^2 and the storage tank volume was larger than 200 m^3, the greenhouse heating load ratio reached more than 100%. The solar collector area required in the combined model was smaller than that determined by the STES model. This difference occurred because the combined model simulates real-time thermal energy supply to the greenhouse based on actual temperature fluctuations, whereas the STES model uses fixed heating load values. This dynamic interaction allows for more efficient utilization of collected STE, resulting in the need for a smaller solar collector area.

Figure 6B shows the selection of the greenhouse pump capacity based on the ratio of the greenhouse heating load according to the pump capacity and the storage tank capacity of the greenhouse. The solar collector area was fixed at 20 m^2. As the storage tank capacity increased, the greenhouse heating load ratio increased, and once it exceeded 100%, it hardly increased further. The greenhouse heating load ratio increased with the pump flow rate and then remained constant due to the storage tank capacity. When the pump flow rate was 3000 kg/h and the storage tank volume was 200 m^3, the greenhouse heating load ratio was 100.3%. When the pump flow rate was changed to 500, 1000, 4000, and 3000 kg/h according to the heat load of each melon growth stage, the results were similar to 3000 kg/h. When the flow rate was changed to 500, 2000, 4000, and 4000 kg/h, similar results were obtained as with 4000 kg/h. Figure 6C shows the heating load ratio according to the pump flow rate, solar collector area, and storage tank volume, comparing the cases where the flow rate was changed to 500, 1000, 4000, and 3000 kg/h for each melon growth stage and where the flow rate was fixed at 5000 kg/h. When the solar collector and storage tank volume were 10-50, the difference in the heating load ratio between the pumps was 0.009, which was almost negligible. The difference was 0.5 at 20-100, 2.4 at 30-150, the highest at 3.7 at 40-200, and decreased to 2.5 at 50-250, after which the difference was maintained. It was confirmed that the heating load ratio between the two flow rates had almost no difference. The heating load ratio of the greenhouse cannot exceed 100% even if the pump flow rate is increased when the storage tank volume is small, so the storage tank volume must first be calculated and the pump flow rate must be calculated to determine the appropriate pump flow rate. In addition, when the pump flow rate is changed according to the crop growth stage, the heating load ratio is not different from operating at a constant flow rate, so heating the greenhouse by changing the pump flow rate can be an economically efficient operating method.

Through the analysis of the greenhouse and STES-combined model, several important design and operational aspects were identified. First, it was found that a smaller solar collector area than determined in the STES model was sufficient to meet the heating load. This is because thermal energy is supplied in real-time according to temperature fluctuations in the greenhouse in the combined model. In contrast, the STES model uses fixed heating load values. This dynamic interaction enables more efficient utilization of collected STE, reducing the required solar collector area. The second relates to the impact of pump flow rate. If the storage tank capacity is sufficient, increasing the pump flow rate above 3000 kg/h did not result in significant changes in the heating load fulfillment ratio. This suggests that the bottleneck in system performance lies in the available storage energy itself rather than the heat transfer rate. In practical implementation, installing oversized pumps would only increase initial and operational costs without contributing to improved system performance. Furthermore, when comparing the strategy of varying pump flow rates according to crop growth stages with operation at a constant flow rate, the difference in heating load fulfillment ratio was minimal. However, the variable flow rate strategy may be more efficient in terms of energy consumption. Particularly, using lower flow rates during periods with less heating demand, such as early growth stages, and higher flow rates during periods with higher heating demand, such as later growth stages, can optimize the power consumption required for pump operation. Finally, the analysis of the relationship between storage tank capacity and solar collector area shows the importance of combining these two elements in system design. When the solar collector area was 20 m^2 and the storage tank capacity was 200 m^3, 100.3% of the greenhouse heating load could be met. This is an important balance point that ensures sufficient capacity while preventing the system from being overdesigned. This is particularly important in the agricultural sector, where initial investment costs can be a major barrier to system adoption, because such optimized designs can improve the economic feasibility of STES systems.

Conclusions

This study determined an appropriate capacity for an STE-based STES system for melon greenhouses by addressing four specific objectives. First, TRNSYS-based energy models were developed for single- and double-layered melon greenhouses using greenhouse properties, crop growth data, growth-stage-specific temperature settings, and weather data. Second, the double-layered greenhouse reduced the mean cumulative cooling and heating loads by 17.8% and 61.6%, respectively, compared with the single-layered greenhouse, owing to its improved insulation performance. Third, as the storage tank heat loss coefficient increased from 0 to 2.0 $kJ/h \cdot m^2 \cdot K$, larger solar collector areas and storage tank volumes were required. Overall, the double-layered greenhouse required 25–50% less solar collector area and 37–60% less storage tank volume than the single-layered greenhouse. Fourth, the integrated greenhouse–STES model showed that a solar collector area of 20 m^2, a storage tank volume of 200 m^3, and a pump flow rate of 3,000 kg/h achieved a winter heating-load fulfillment ratio of 100.3% for the single-layered greenhouse. Increasing the pump flow rate above 3,000 kg/h provided little additional benefit. These findings provide a simulation-based approach for appropriately sizing STES systems and can support reductions in system overdesign, fossil fuel consumption, and greenhouse gas emissions in melon greenhouse production.

References

Abbouda SK, Almuhanna EA, Al-Amri AM, 2012. Effect of using double layers of polyethylene cover with air gap on control environment inside greenhouses. Proc. Annual ASABE Int. Meet., Dallas; paper 121341057.

Adesanya MA, Rabiu A, Ogunlowo QO, Kim M-H, Akpenpuun TD, Na WH, et al., 2025. Experimental evaluation of hybrid renewable and thermal energy storage systems for a net-zero energy greenhouse: a case study of Yeoju-Si. Energies 18:1-23.

Ahamed MS, Guo H, Tanino K, 2020. Modeling heating demands in a Chinese-style solar greenhouse using the transient building energy simulation model TRNSYS. J Build Eng 29:101114.

Allen M, Dube OP, Solecki W, Aragón-Durand F, Cramer W, Humphreys S, Kainuma M, 2018. Special report: Global warming of 1.5 C. Intergovernmental Panel on Climate Change (IPCC). Available from: https://www.ipcc.ch/sr15/

Aljubury IMA, Ridha HD, 2017. Enhancement of evaporative cooling system in a greenhouse using geothermal energy. Renew Energy 111:321-31.

Antonanzas J, Osorio N, Escobar R, Urraca R, Martinez-de-Pison FJ, Antonanzas-Torres F, 2016. Review of photovoltaic power forecasting. Solar Energy 136:78-111.

Anwar MN, Iftikhar M, Khush Bakhat B, Sohail NF, Baqar M, Yasir A, Nizami AS, 2020. Sources of carbon dioxide and environmental issues. In: Inamuddin, Asiri A, Lichtfouse E (eds), Carbon sequestration. Introduction and biochemical methods. Cham, Springer; pp. 13-36.

Attar I, Naili N, Khalifa N, Hazami M, Farhat A, 2013. Parametric and numerical study of a solar system for heating a greenhouse equipped with a buried exchanger. Energy Convers Manag 70:163-73.

Beaulac A, Lalonde T, Haillot D, Monfet D, 2024. Energy modeling, calibration, and validation of a small-scale greenhouse using TRNSYS. Appl Therm Eng 248:123195.

Çam NY, Ezan MA, Biçer Y, 2024. An integrated transient model in TRNSYS for thermal management of the tomato growth process in a greenhouse with a PV-aided heat pump-assisted HVAC system. Int J Thermofluids 22:100592.

Chung M, Park JU, Yoon HK, 1998. Simulation of a central solar heating system with seasonal storage in Korea. Solar Energy 64:163-178.

Dahash A, Ochs F, Janetti MB, Streicher W, 2019. Advances in seasonal thermal energy storage for solar district heating applications: A critical review on large-scale hot-water tank and pit thermal energy storage systems. Appl Energy 239:296-315.

Dolgun GK, Keçebaş A, Ertürk M, Daşdemir A, 2023. Optimal insulation of underground spherical tanks for seasonal thermal energy storage applications. J Energy Storage 69:107865.

Esen M, Yuksel T, 2013. Experimental evaluation of using various renewable energy sources for heating a greenhouse. Energy Build 65:340-51.

Filonchyk M, Peterson MP, Zhang L, Hurynovich V, and He Y, 2024. Greenhouse gases emissions and global climate change: Examining the influence of CO2, CH4, and N2O. Sci Total Environ 935:173359.

Fisch MN, Guigas M, Dalenbäck JO, 1998. A review of large-scale solar heating systems in Europe. Solar Energy 63:355-66.
Goo J, Shin H, Kwak Y, Huh J, 2021. Development of smart greenhouse energy analysis model and analysis of cooling packages performance. J Korean Solar Energy Society 41:1-18.
Ha T, Lee IB, Kwon KS, Hong SW, 2015. Computation and field experiment validation of greenhouse energy load using building energy simulation model. Int J Agric Biol Eng 8:116-27.
Hassanien RHE, Li M, Lin WD, 2016. Advanced applications of solar energy in agricultural greenhouses. Renew Sustain Energ Rev 54:989-1001.
Höök M, Tang X, 2013. Depletion of fossil fuels and anthropogenic climate change - A review. Energ Policy 52:797-809.
Hussain MI, Ali A, Lee GH, 2015. Performance and economic analyses of linear and spot Fresnel lens solar collectors used for greenhouse heating in South Korea. Energy 90:1522-31.
Iddio E, Wang L, Thomas Y, McMorrow G, Denzer A, 2020. Energy efficient operation and modeling for greenhouses: A literature review. Renew Sustain Energ Rev 117:109480.
International Energy Agency (IEA), 2023. CO2 Emissions in 2022. Available from: https://www.iea.org/reports/co2-emissions-in-2022
Jabloun Md, Sahli A, 2008. Evaluation of FAO-56 methodology for estimating reference evapotranspiration using limited climatic data: Application to Tunisia. Agric Water Manage 95:707-15.
Kesh H, Kaushik P, 2021. Advances in melon (Cucumis melo L.) breeding: An update. Sci Hortic 282:110045.
Kim D, Lee D, Heo J, Kim MH, 2022. Analysis of greenhouse gas and operation cost reduction effect of a solar thermal-based renewable energy convergence system greenhouse. Korean J Air-Cond Refrig Eng 34:447-55.
Lee M, Lee I, Ha T, Kim R, Yeo U, Lee S, et al., 2017. Estimation on heating and cooling loads for a multi-span greenhouse and performance analysis of pv system using building energy simulation. J Bio-Env Con 26:258-67.
Lee S, Lee I, Homg S, Seo I, Bitog PJ, Kwon K, et al., 2012. Prediction of greenhouse energy loads using building energy simulation (bes). J Korean Soc Agric Eng 54:113-24.
Lee S, Park S, Lee I, Ha T, Kwon K, Kim R, et al., 2016. Design of energy model of greenhouse including plant and estimation of heating and cooling loads for a multi-span plastic-film greenhouse by building energy simulation. J Bio-Env Con 25:123-32.
Nam S, Kim Y, Seo D, 2024. Change in the plant temperature of tomato by fogging and airflow in plastic greenhouse. J Bio-Env Con 23:11-8.
Ogunlowo QO, Akpenpuun TD, Na WH, Adesanya MA, Rabiu A, Dutta P, et al., 2023. Simulation of greenhouse energy and strawberry (Seolhyang sp.) yield using TRNSYS DVBES: A base case. Solar Energy 266:112196.
Park J, Kim Y, 2019. The effects of renewable energy in agricultural sector. J Korea Acad-Indl Coop Soc 20:224-35. https://doi.org/10.5762/KAIS.2019.20.1.224
Park S, 2023. Calculation of cooling/heating loads and seasonal thermal energy storage

system capacity for melon greenhouse using energy analysis program. Available from: https://www.goveda.com/patent/KR-20250119819-A

Rabiu A, Na W, Akpenpuun TD, Rasheed A, Adesanya MA, Ogunlowo QO, et al., 2022. Determination of overall heat transfer coefficient for greenhouse energy-saving screen using Trnsys and hotbox. Biosyst Eng217:83-101.

Rasheed A, Kwak CS, Na WH, Lee JW, Kim HT, Lee HW, 2020. Development of a building energy simulation model for control of multi-span greenhouse microclimate. Agronomy 10:1236.

Roble C, 2019. Global Greenhouse Statistics 2019. Available from: https://www.producegrower.com/news/cuesta-roble-2019-global-greenhouse-statistics/

Semple L, Carriveau R, Ting DS, 2017. A techno-economic analysis of seasonal thermal energy storage for greenhouse applications. Energy Build 154:175-87.

Stanghellini C, 1987. Transpiration of greenhouse crops: an aid to climate management. Wageningen University and Research. Available from: https://research.wur.nl/en/publications/transpiration-of-greenhouse-crops-an-aid-to-climate-management/

Transsolar Energietechnik GmbH, 2019. Multizone Building modeling with Type56 and TRNBuild. TRNSYS 18 Documentation 5:162-163.

Trépanier M, Schwarz P, Gosselin L, 2024. Simulating the impact of climate change on energy consumption and yield in Canadian greenhouse horticulture. Sustain Futures 8:100354.

Trier D, 2012. Solar district heating guidelines. Fact sheet 7.2:1-13.

Xu J, Wang RZ, Li Y, 2014. A review of available technologies for seasonal thermal energy storage. Solar Energy

Zhang L, Xu P, Mao J, Tang X, Li Z, Shi J, 2015. A low cost seasonal solar soil heat storage system for greenhouse heating: Design and pilot study. Appl Energy 156:213-22.

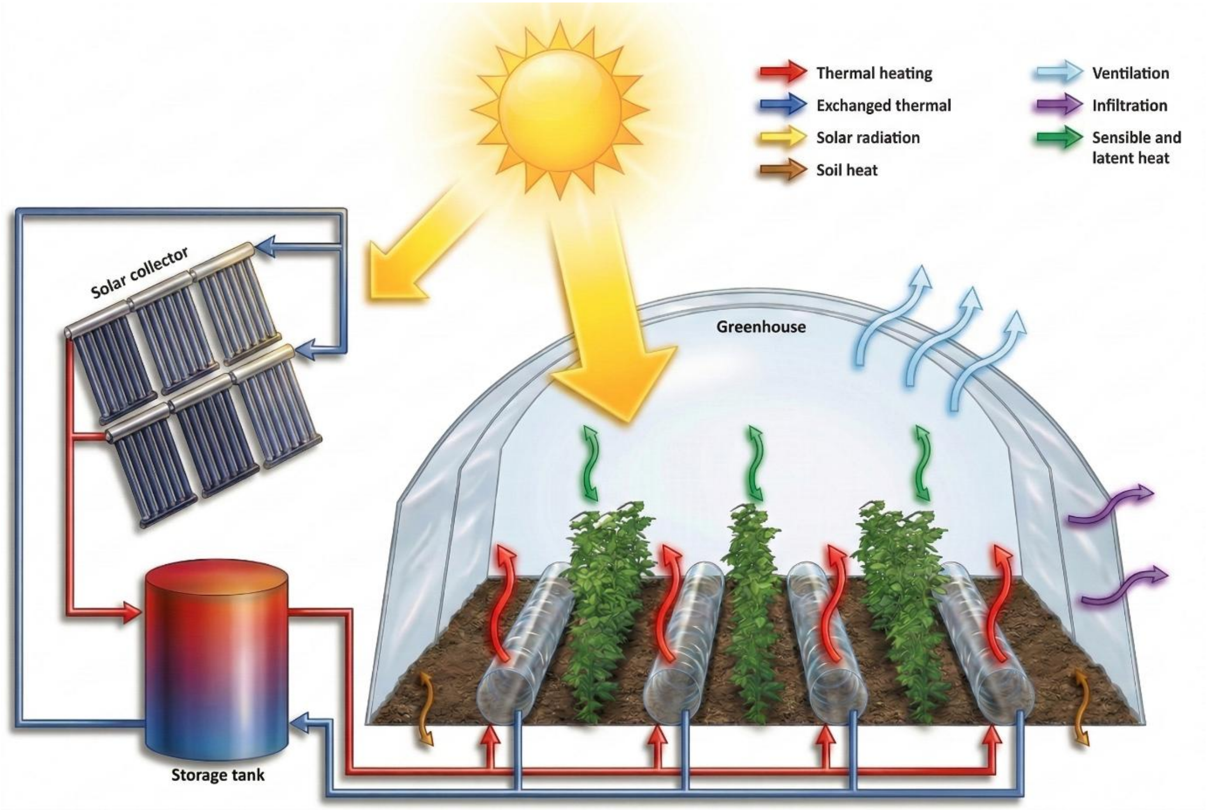

Figure 1. Schematic diagram of the STES system and greenhouse energy flow. The diagram shows the energy flows associated with solar radiation, soil heat transfer, ventilation, infiltration, crop sensible and latent heat, heating energy, and heat exchange between the STES and the greenhouse. TRNSYS simulations were performed to calculate the greenhouse heating and cooling loads and to estimate the required STES capacity based on these energy flows.

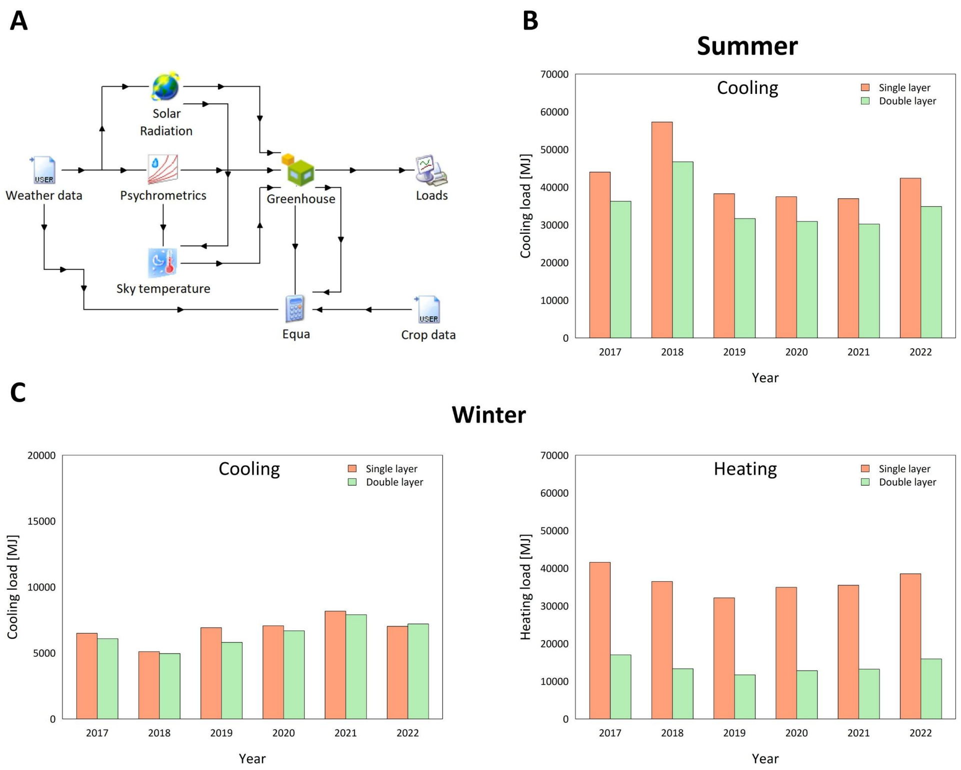

Figure 2. TRNSYS analysis using greenhouse models for cooling and heating load calculation. (A) TRNSYS model for greenhouse thermal energy analysis using weather and crop data. (B) Cooling loads of the single- and double-layered greenhouses during the summer cropping seasons over the six-year simulation period. (C) Heating and cooling loads of the single- and double-layered greenhouses during the winter cropping seasons over the six-year simulation period.

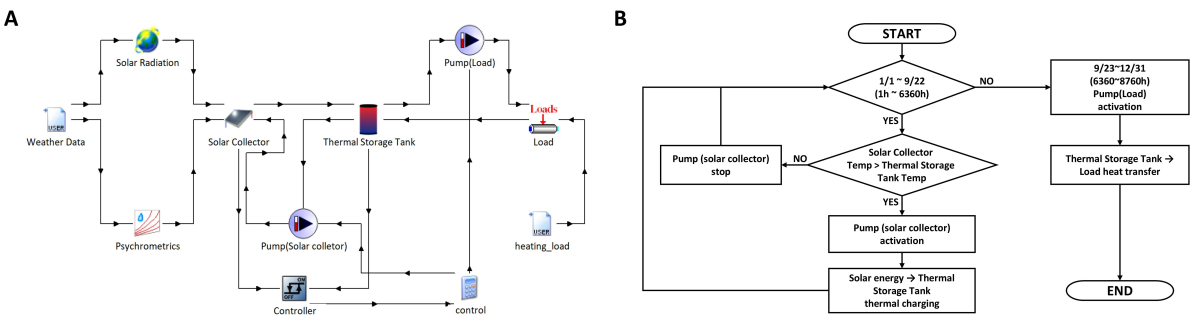

Figure 3. Configuration and operation flowchart of the STES model. (A) TRNSYS-based STES model using the heating load calculated from the greenhouse model. (B) Flowchart of the STES model operation.

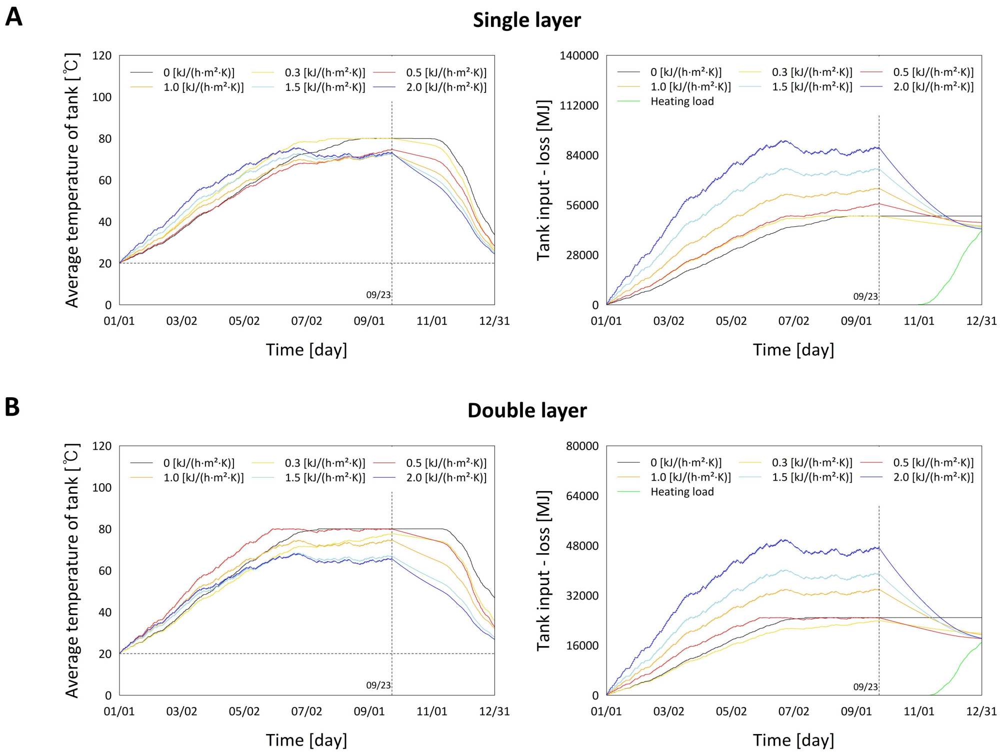

Figure 4. STES capacity according to the storage tank heat loss coefficient. (A) Average storage tank temperature and the difference between energy input and heat loss according to the storage tank heat loss coefficient in the single-layered greenhouse. (B) Average storage tank temperature and the difference between energy input and heat loss according to the storage tank heat loss coefficient in the double-layered greenhouse.

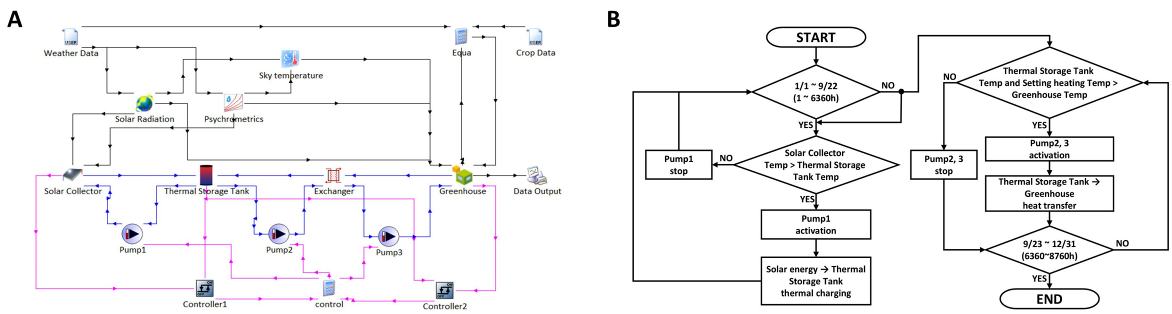

Figure 5. Configuration and operation flowchart of the integrated greenhouse–STES model. (A) Combined STES–greenhouse model for estimating the required STES capacity. (B) Flowchart of the combined STES–greenhouse model.

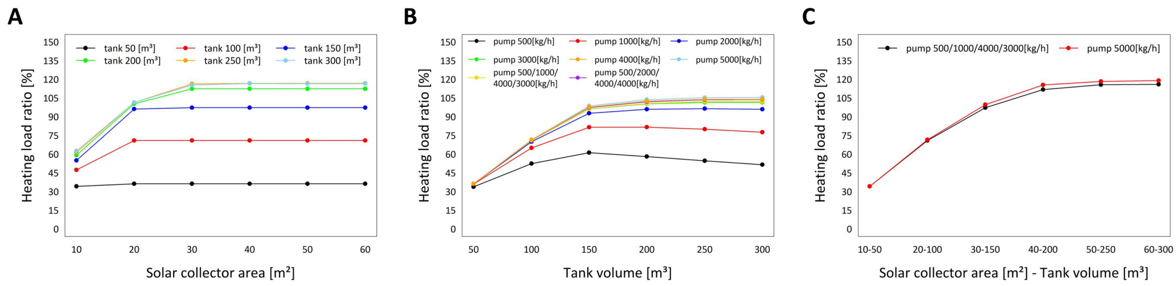

Figure 6. Heating load fulfillment ratio of the integrated greenhouse–STES model according to system capacity and pump flow rate. (A) Fulfillment ratio of the greenhouse heating load according to solar collector area and storage tank volume. (B) Greenhouse heating load ratio according to greenhouse pump flow rate and storage tank volume. (C) Heating load ratio according to pump flow rate, solar collector area, and storage tank volume.

Table 1. The physical properties of wall and floor used in the greenhouse model.

Materials		Density (kg/m³)	Specific heat (kJ/kg·K)	Thermal conductivity (kJ/h·m·K)	Thickness (m)
Wall	Aluminum alloy	2700	0.88	730	0.18
	Concrete	2240	0.92	6.23	0.3
Floor	Gravel	1800	1	7.2	0.2
	Sand	2240	0.92	6.29	0.35

Table 2. The physical properties of cladding material used in the greenhouse model.

Materials	Solar transmittance	Solar reflectance	Visible transmittance	Visible reflectance	Infrared emittance	Thermal conductivity (kJ/h·m·K)	Thickness (mm)
PE	0.75	0.1	0.88	0.1	0.84	1.19	0.1

Table 3. Setting temperature of the greenhouse according to melon growth stage.

Growth stage	Cropping Season		Setting temperature (°C)	
	Summer	Winter	Heating	Cooling
Planting - Fruit bearing	05/24-07/07	09/23-11/06	14	28
Fruit growing period	07/08-07/17	11/07-11/16	18	30
Fruit net growing period	07/18-08/11	11/17-12/11	18	35
Maturation - Harvesting	08/12-08/31	12/12-12/31	14	28

Table 4. Values of the parameters of the various $\tilde{r}_i$ functions, as a result of the optimization program (Stanghellini, 1987).

Equation	Parameters	Daytime	Nighttime	Unit
	r_{min}	82.0	658.5	$s \bullet m^{-1}$
$\tilde{r}_i(I_s)$	C_1	4.30		$W \bullet m^{-2}$
	C_2	0.54		$W \bullet m^{-2}$
$\tilde{r}_i(T_0)$	C_3	2.3×10^{-2}	0.5×10^{-2}	K^{-2}
	T_m	24.5	33.6	℃
$\tilde{r}_i(CO_2)$	C_4	6.1×10^{-7}	1.1×10^{-11}	vpm^{-2}
$\tilde{r}_i(e_E - e_a)$	C_5	4.3	5.2	kPa^{-2}

Table 5. Annual cumulative cooling and heating loads and maximum hourly loads with occurrence dates for single- and double-layered melon greenhouses by cropping season and growth stage during 2017–2022.

Layer	Season	Stage	Load type	Year (MJ)						
				2017	**2018**	**2019**	**2020**	**2021**	**2022**	**Mean ± SD**
Single	Summer	1	Cooling	26,716.27	25,373.69	23,141.84	20,801.13	20,978.91	28,222.88	24,206 ± 3,064
			Heating	-	-	-	-	-	-	-
		2	Cooling	3,198.67	6,836.17	2,056.51	1,445.32	4,321.20	3,765.37	3,604 ± 1,908
			Heating	-	-	-	-	-	-	-
		3	Cooling	5,663.33	11,903.79	4,003.66	450.88	5,665.75	2,662.28	5,058 ± 3,890
			Heating	-	-	-	-	-	-	-
		4	Cooling	8,391.92	13,144.25	9,041.00	14,758.60	6,004.18	7,734.10	9,846 ± 3,376
			Heating	-	-	-	-	-	-	
		Total	Cooling	43,970.19	57,257.90	38,243.01	37,455.93	36,970.04	42,384.63	42,714 ± 7,666
			Heating	-	-	-	-	-	-	-
		Maximum (MJ/h)	Cooling (date)	137.04 (06/18)	142.19 (06/02)	137.88 (05/24)	142.50 (06/10)	129.81 (06/08)	143.26 (05/24)	-
			Heating (date)	-	-	-	-	-	-	-
	Winter	1	Cooling	6,499.72	5,112.75	6,926.31	7,070.26	8,126.38	6,998.19	6,789 ± 982
			Heating	697.30	841.06	46.97	626.63	578.72	507.80	550 ± 271
		2	Cooling	-	-	-	-	46.83	24.32	36 ± 16
			Heating	3,590.34	3,562.18	3,721.64	3,309.46	5,161.62	2,713.97	3,677 ± 811
		3	Cooling	-	-	-	-	-	-	-
			Heating	21,923.43	18,285.14	16,461.11	16,187.26	15,990.64	15,132.68	17,330 ± 2,478
		4	Cooling	-	-	-	-	-	-	-
			Heating	15,365.94	13,803.29	11,921.05	14,813.71	13,755.90	20,189.27	14,975 ± 2,813
		Total	Cooling	6,499.72	5,112.75	6,926.31	7,070.26	8,173.21	7,022.51	6,801 ± 996
			Heating	41,577.01	36,491.67	32,150.77	34,937.06	35,486.88	38,543.72	36,531 ± 3,235
		Maximum (MJ/h)	Cooling (date)	110.77 (09/26)	83.79 (09/25)	80.52 (09/23)	95.77 (09/28)	106.24 (10/06)	99.69 (09/30)	-
			Heating (date)	79.05 (12/05)	88.52 (12/09)	81.20 (12/06)	84.43 (12/31)	82.97 (12/26)	86.13 (12/25)	-
Double	Summer	1	Cooling	25,167.92	23,581.03	21,231.31	19,352.78	19,772.95	25,793.41	22,483 ± 2,760
			Heating	-	-	-	-	-	-	-
		2	Cooling	1,828.44	4,428.63	1,187.06	643.06	2,632.05	2,475.08	2,199 ± 1,328
			Heating	-	-	-	-	-	-	-
		3	Cooling	2,889.31	8,582.17	2,150.59	60.50	3,324.26	1,105.07	3,019 ± 2,974
			Heating	-	-	-	-	-	-	-
		4	Cooling	6,373.59	10,135.23	7,111.43	10,855.85	4,461.98	5,505.13	7,407 ± 2,561
			Heating	-	-	-	-	-	-	-
		Total	Cooling	36,259.26	46,727.06	31,680.39	30,912.19	30,191.24	34,878.69	35,108 ± 6,163
			Heating	-	-	-	-	-	-	-
		Maximum (MJ/h)	Cooling (date)	95.86 (05/25)	91.79 (05/26)	99.25 (05/24)	89.34 (06/10)	82.69 (06/08)	104.94 (05/24)	-
			Heating (date)	-	-	-	-	-	-	-
	Winter	1	Cooling	6,093.72	4,955.71	5,803.35	6,692.86	7,904.65	7,209.03	6,443 ± 1,052
			Heating	-	-	-	-	-	-	-
		2	Cooling	-	-	-	-	-	-	-
			Heating	545.43	634.45	518.20	483.52	1,663.82	248.68	682 ± 498
		3	Cooling	-	-	-	-	-	-	-
			Heating	9,668.30	7,211.35	6,195.72	6,330.56	6,372.73	5,657.63	6,906 ± 1,442
		4	Cooling	-	-	-	-	-	-	-
			Heating	6,798.26	5,499.31	5,000.13	6,023.81	5,188.43	10,027.74	6,423 ± 1,881
		Total	Cooling	6,093.72	4,955.71	5,803.35	6,692.86	7,904.65	7,209.03	6,443 ± 1,052
			Heating	17,011.99	13,345.11	11,714.05	12,837.89	13,224.98	15,934.05	14,011 ± 2,021
		Maximum (MJ/h)	Cooling (date)	75.00 (09/26)	62.97 (09/25)	66.34 (09/23)	67.31 (09/28)	83.70 (09/23)	79.89 (09/24)	-
			Heating (date)	42.61 (12/05)	48.72 (12/09)	42.07 (12/06)	44.42 (12/31)	42.16 (12/26)	49.97 (12/24)	-

Table 6. Comparison of solar collector and storage tank capacity and integrated energy according to the loss coefficient of storage tank (single and double-layered greenhouse)

Layer	Storage tank loss coefficient (kJ/h·m²·K)	Solar collector area (m²)	Storage tank volume (m³)	Energy [MJ]				
				Solar collector	Storage tank			Heating load
					Input (A)	Loss (B)	A-B	
Single	0	30	200	50,022	49,799	-	49,799	41,558
	0.3	40	200	64,694	64,374	20,674	43,700	
	0.5	40	250	80,506	80,162	33,973	46,189	
	1	60	300	121,039	120,635	76,393	44,242	
	1.5	90	350	175,077	174,665	131,238	43,426	
	2	130	400	241,533	241,053	198,486	42,567	
Double	0	20	100	25,076	24,902	-	24,902	17,003
	0.3	20	100	32,664	32,356	12,461	19,895	
	0.5	30	100	42,316	42,015	23,832	18,182	
	1	40	150	72,933	72,718	53,297	19,421	
	1.5	50	200	101,182	100,954	82,726	18,228	
	2	70	250	143,428	143,150	124,908	18,242	